A Physically-Based Statistical Deformable Model for Brain Image Analysis

Christophoros Nikou[1,2], Fabrice Heitz[1], Jean-Paul Armspach[2], and Gloria Bueno[1,2]

[1] Laboratoire des Sciences de l'Image de l'Informatique et de la Télédétection
Université Strasbourg I (UPRES-A CNRS 7005)
4, boulevard Sébastien Brant, 67400 Illkirch, France
[2] Institut de Physique Biologique, Faculté de Médecine
Université Strasbourg I (UPRES-A CNRS 7004)
4, rue Kirschleger, 67085 Strasbourg CEDEX, France

Abstract. A probabilistic deformable model for the representation of brain structures is described. The statistically learned deformable model represents the relative location of head (skull and scalp) and brain surfaces in Magnetic Resonance Images (MRIs) and accommodates their significant variability across different individuals. The head and brain surfaces of each volume are parameterized by the amplitudes of the vibration modes of a deformable spherical mesh. For a given MRI in the training set, a vector containing the largest vibration modes describing the head and the brain is created. This random vector is statistically constrained by retaining the most significant variation modes of its Karhunen-Loeve expansion on the training population. By these means, the conjunction of surfaces are deformed according to the anatomical variability observed in the training set. Two applications of the probabilistic deformable model are presented: the deformable model-based registration of 3D multimodal (MR/SPECT) brain images without removing non-brain structures and the segmentation of the brain in MRI using the probabilistic constraints embedded in the deformable model. The multi-object deformable model may be considered as a first step towards the development of a general purpose probabilistic anatomical brain atlas.

1 Introduction

In medical image analysis, deformable models offer a unique and powerful approach to accommodate the significant variability of biological structures over time and across different individuals. A survey on deformable models as a promising computer-assisted medical image analysis technique has recently been presented in [7].

We present a 3D statistical deformable model carrying information on multiple anatomical structures (head -skull and scalp- and brain) for multimodal brain image processing. Our goal is to describe the spatial relation between these anatomical structures as well as the shape variations observed over a representative

D. Vernon (Ed.): ECCV 2000, LNCS 1843, pp. 528–542, 2000.
© Springer-Verlag Berlin Heidelberg 2000

population of individuals. In our approach, the different anatomical structures are represented by physics-based deformable models [13] whose parameters undergo statistical training. The resulting joint statistical deformable model is considered as a first step towards the development of a general purpose probabilistic atlas for various applications in medical image analysis (segmentation, labeling, registration, pathology characterization).

In the proposed approach the considered anatomical structures surfaces are extracted from a training set of 3D MRI. These surfaces are then parameterized by the amplitudes of the vibration modes of a physically-based deformable model [13,10] and a joint model is constructed for each set of structures. The joint model is then statistically constrained by a Karhunen-Loeve decomposition of the vibration modes. By these means, the spatial relation between the head and brain structures, as well as the anatomical variability observed in the training set are compactly described by a limited number of parameters.

Physics-based models enable a hierarchical description of anatomical structures as the ordered superimposition of vibrations (of different frequencies) of an initial mesh. Physically-based parameterizations are also invariant to *small* misregistration in rotation (contrary to Point Distribution Models (PDMs) [4], needing accurate rotation and translation compensation). Let us notice that physically-based models also differ from 3D Fourier descriptors because the latter also need a uniform way to discretize the surface and are not rotation invariant [14].

Two applications of the probabilistic deformable model are presented in this paper:

- The segmentation of the brain from MRIs using the probabilistic constraints embedded in the deformable model.
- The robust deformable model-based rigid registration of 3D multimodal (MR/SPECT) brain images by optimizing an energy function relying on the chamfer distance between the statistically constrained model parts and the image data.

The remainder of this paper is organized as follows: in Section 2, the parameterization of the head and brain structures by the vibration modes of a spherical mesh is presented. The statistical training procedure is described in Section 3. The applications of the probabilistic model to 3D segmentation and to multimodal (MRI/SPECT) image registration are presented in Section 4. Experimental results on real data, with a 50-patients trained model, are presented and commented on in the same section. Finally, conclusions are proposed in Section 5.

2 3D Physics-Based Deformable Modeling

To provide a training set, a representative collection of 50 3D MRI volumes of different patients have first been registered to a reference image using an unsupervised robust rigid registration technique [11,12]. This preliminary step is

necessary to provide a consistent initialization for the deformable model for all images in the training step, since the representation is not invariant to rotation (the same alignment is also applied to the patient data processed in Section 4). The head of each volume has then been segmented by simple thresholding and region growing [9].

Both head and brain contours were parameterized by the amplitudes of the vibration modes of a physics-based deformable model. Following the approach of Nastar *et al.* [10], the model for a given structure consists of 3D points sampled on a spherical surface, following a quadrilateral cylinder topology in order to avoid singularities due to the poles. Each node has a mass m and is connected to its four neighbours with springs of stiffness k. The model nodes are stacked in vector:

$$\mathbf{X}_0 = (x_1^0, y_1^0, z_1^0, ..., x_{N'N}^0, y_{N'N}^0, z_{N'N}^0)^T \tag{1}$$

where N is the number of points in the direction of the geographical longitude and N' is the number of points in the direction of the geographical latitude of the sphere. The physical model is characterized by its mass matrix $\mathbf{M}$, its stiffness matrix $\mathbf{K}$ and its dumping matrix $\mathbf{C}$ and its governing equation may be written as [13]:

$$\mathbf{M}\ddot{\mathbf{U}} + \mathbf{C}\dot{\mathbf{U}} + \mathbf{K}\mathbf{U} = \mathbf{F} \tag{2}$$

where $\mathbf{U}$ stands for the nodal displacements of the initial mesh $\mathbf{X}_0$. The image force vector $\mathbf{F}$ is based on the euclidean distance between the mesh nodes and their nearest contour points [3].

Since equation (2) is of order $3NN'$, where NN' is the total number of nodes of the spherical mesh, it is solved in a subspace corresponding to the truncated vibration modes of the deformable structure [10,13], using the following change of basis:

$$\mathbf{U} = \mathbf{\Phi}\tilde{\mathbf{U}} = \sum_i \tilde{u}_i \phi_i, \tag{3}$$

where $\mathbf{\Phi}$ is a matrix and $\tilde{\mathbf{U}}$ is a vector, ϕ_i is the ith column of $\mathbf{\Phi}$ and $\tilde{u}_i$ is the ith scalar component of vector $\tilde{\mathbf{U}}$. By choosing $\mathbf{\Phi}$ as the matrix whose columns are the eigenvectors of the eigenproblem:

$$\mathbf{K}\phi_i = \omega_i^2 \mathbf{M}\phi_i, \tag{4}$$

and using the standard Rayleigh hypothesis [10], matrices $\mathbf{K}$, $\mathbf{M}$ and $\mathbf{C}$ are simultaneously diagonalized:

$$\begin{cases} \mathbf{\Phi}^T\mathbf{M}\mathbf{\Phi} = \mathbf{I} \\ \mathbf{\Phi}^T\mathbf{K}\mathbf{\Phi} = \mathbf{\Omega}^2 \end{cases} \tag{5}$$

where $\mathbf{\Omega}^2$ is the diagonal matrix whose elements are the eigenvalues ω_i^2 and $\mathbf{I}$ is the identity matrix.

An important advantage of this formulation is that the eigenvectors and the eigenvalues of a quadrilateral mesh with cylinder topology have an explicit

expression [1] and they do not have to be computed by standard slow eigen-decomposition techniques (generally matrices $\mathbf{K}$ and $\mathbf{M}$ are very large). The eigenvalues are given by the equation:

$$\omega_{p,p'}^2 = \frac{4k}{m}\left(\sin^2\frac{p\pi}{2N} + \sin^2\frac{p'\pi}{N'}\right) \tag{6}$$

and the eigenvectors are obtained by:

$$\phi_{p,p'} = \left[..., \cos\frac{(2n-1)p\pi}{2N}\cos\frac{2n'p'\pi}{N'}, ...\right]^T \tag{7}$$

with $n \in \{1, 2, ..., N\}$ and $n' \in \{1, 2, ..., N'\}$.

Substituting (3) into (2) and premultiplying by $\mathbf{\Phi}^T$ yields:

$$\ddot{\tilde{\mathbf{U}}} + \tilde{\mathbf{C}}\dot{\tilde{\mathbf{U}}} + \mathbf{\Omega}^2\tilde{\mathbf{U}} = \tilde{\mathbf{F}} \tag{8}$$

where $\tilde{\mathbf{C}} = \mathbf{\Phi}^T\mathbf{C}\mathbf{\Phi}$ and $\tilde{\mathbf{F}} = \mathbf{\Phi}^T\mathbf{F}$.

In many computer vision applications [13], when the initial and the final state are known, it is assumed that a constant load $\mathbf{F}$ is applied to the body. Thus, equation (2) is called the equilibrium governing equation and corresponds to the static problem:

$$\mathbf{K}\mathbf{U} = \mathbf{F} \tag{9}$$

In the new basis, equation (9) is thus simplified to $3NN'$ scalar equations:

$$\omega_i^2\tilde{u}_i = \tilde{f}_i. \tag{10}$$

In equation (10), ω_i designates the ith eigenvalue, the scalar $\tilde{u}_i$ is the amplitude of the corresponding vibration mode (corresponding to eigenvector ϕ_i). Equation (10), indicates that instead of computing the displacements vector $\mathbf{U}$ from equation (9), we can compute its decomposition in terms of the vibration modes of the original mesh.

The number of vibration modes retained in the object description, is chosen so as to obtain a compact but adequately accurate representation. A typical *a priori* value covering many types of standard deformations is the quarter of the number of degrees of freedom in the system [10] (i.e. 25% of the modes are kept). Figure 1 shows the parameterization of head and brain surfaces considered for a subject belonging to the training set, by the 25% lowest frequency modes. Although not providing a high resolution description of the brain surface, this truncated representation provides a satisfactory compromise between accuracy and complexity of the representation. The spherical model is initialized around the structures of interest (fig. 1(a) and 1(d)). The vibration amplitudes are explicitly computed by equation (10), where rigid body modes ($\omega_i = 0$) are discarded and the nodal displacements may be recovered using equation (3). The physical representation $\mathbf{X}(\tilde{\mathbf{U}})$ is finally given by applying the deformations to the initial spherical mesh (fig. 1(b-c) and 1(e-f)):

$$\mathbf{X}(\tilde{\mathbf{U}}) = \mathbf{X}_0 + \mathbf{\Phi}\tilde{\mathbf{U}} \tag{11}$$

Thus, the head and brain surfaces of a particular patient are hierarchically described in terms of vibrations of an initial spherical mesh. The next step consists in applying the above parameterization to each patient of the training set and to perform statistical learning for the head and brain structures.

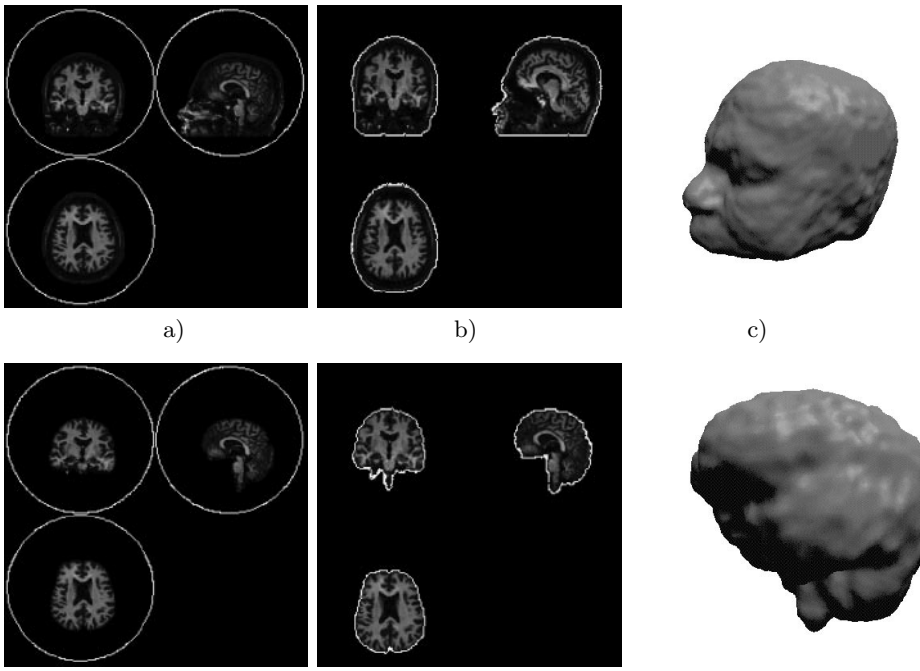

Fig. 1. *Head and brain parameterization from 3D MRI. The first column shows in a multiplanar (sagittal, coronal, transversal) view the initial spherical mesh superimposed to the structures to be parameterized. The midlle column presents in a multiplanar view the deformable models at equilibrium (25% of the modes). The last column illustrates 3D renderings of the physically-based models. The rows from top to bottom correspond to:* **(a)-(c)** *head and* **(d)-(f)** *brain.*

3 Statistical Training: The Joint Model

For each image $i = 1, ..., n$ $(n = 50)$ in the training set, a vector $\mathbf{a}_i$containing the lowest frequency vibration modes, M_H and M_B, describing the head and the brain, respectively, is created:

$$\mathbf{a}_i = (\tilde{\mathbf{U}}_i^H, \tilde{\mathbf{U}}_i^B)^T \tag{12}$$

where:

$$\tilde{\mathbf{U}}_i^H = (\tilde{u}_1^h, \tilde{u}_2^h, \ldots, \tilde{u}_{M_H}^h)_i \tag{13}$$

$$\tilde{\mathbf{U}}_i^B = (\tilde{u}_1^b, \tilde{u}_2^b, \ldots, \tilde{u}_{M_B}^b)_i \tag{14}$$

with $3(M_H + M_B) < 6NN'$.

Random vector $\mathbf{a}$ is statistically constrained by retaining the most significant variation modes in its Karhunen-Loeve (KL) transform [4,5]:

$$\mathbf{a} = \bar{\mathbf{a}} + \mathbf{P}\mathbf{b} \tag{15}$$

where

$$\bar{\mathbf{a}} = \frac{1}{n}\sum_{i=1}^{n} \mathbf{a}_i \tag{16}$$

is the average vector of vibration amplitudes of the structures belonging to the training set, $\mathbf{P}$ is the matrix whose columns are the eigenvectors of the covariance matrix

$$\mathbf{\Gamma} = \mathbb{E}\left[(\mathbf{a} - \bar{\mathbf{a}})^T(\mathbf{a} - \bar{\mathbf{a}})\right] \tag{17}$$

and

$$\mathbf{b}_i = \mathbf{P}^T(\mathbf{a}_i - \bar{\mathbf{a}}) \tag{18}$$

are the coordinates of $(\mathbf{a} - \bar{\mathbf{a}})$ in the eigenvector basis.

The deformable model is finally parameterized by the m most significant statistical deformation modes stacked in vector $\mathbf{b}$. By modifying $\mathbf{b}$, both head and brain are deformed in conjunction (fig. 2), according to the anatomical variability observed in the training set. The multi-object deformable model describes the spatial relationships between the considered surfaces of a subject as well as their shape variations.

Given the double (head and brain) initial spherical mesh:

$$\mathbf{X}_{INIT} = \begin{pmatrix} \mathbf{X}_0 \\ \mathbf{X}_0 \end{pmatrix}, \tag{19}$$

the statistical deformable model $\mathbf{X}(\mathbf{a})$ is thus represented by:

$$\mathbf{X}(\mathbf{a}) = \mathbf{X}_{INIT} + \underline{\overline{\mathbf{\Phi}}}\mathbf{a} \tag{20}$$

Combining equations (15) and (20) we have:

$$\mathbf{X}(\mathbf{b}) = \mathbf{X}_{INIT} + \underline{\overline{\mathbf{\Phi}}}\bar{\mathbf{a}} + \underline{\overline{\mathbf{\Phi}}}\mathbf{P}\mathbf{b} \tag{21}$$

where:

$$\underline{\overline{\mathbf{\Phi}}} = \begin{pmatrix} \mathbf{\Phi}_H & \mathbf{0} \\ \mathbf{0} & \mathbf{\Phi}_B \end{pmatrix}, \quad \mathbf{P} = \begin{pmatrix} \mathbf{P}_{HB} \\ \mathbf{P}_{BH} \end{pmatrix}, \quad \bar{\mathbf{a}} = \begin{pmatrix} \bar{\mathbf{a}}_H \\ \bar{\mathbf{a}}_B \end{pmatrix} \tag{22}$$

In equation (22), the columns of the $3NN' \times 3M_H$ matrix $\mathbf{\Phi}_H$ are the eigenvectors of the spherical mesh describing the head surface and the columns of the $3NN' \times 3M_B$ matrix $\mathbf{\Phi}_B$ are the eigenvectors of the spherical mesh describing

the brain surface. Besides, the $3M_H \times m$ matrix $\mathbf{P}_{HB}$ and the $3M_B \times m$ matrix $\mathbf{P}_{BH}$ describe the statistical dependencies of head and brain deformations observed in the training set. Vectors $\bar{\mathbf{a}}_H$ and $\bar{\mathbf{a}}_B$ are of order $3M_H \times 1$ and $3M_B \times 1$ respectively, and vector $\mathbf{b}$ has a low dimension $m \ll 3\,(M_H + M_B)$.

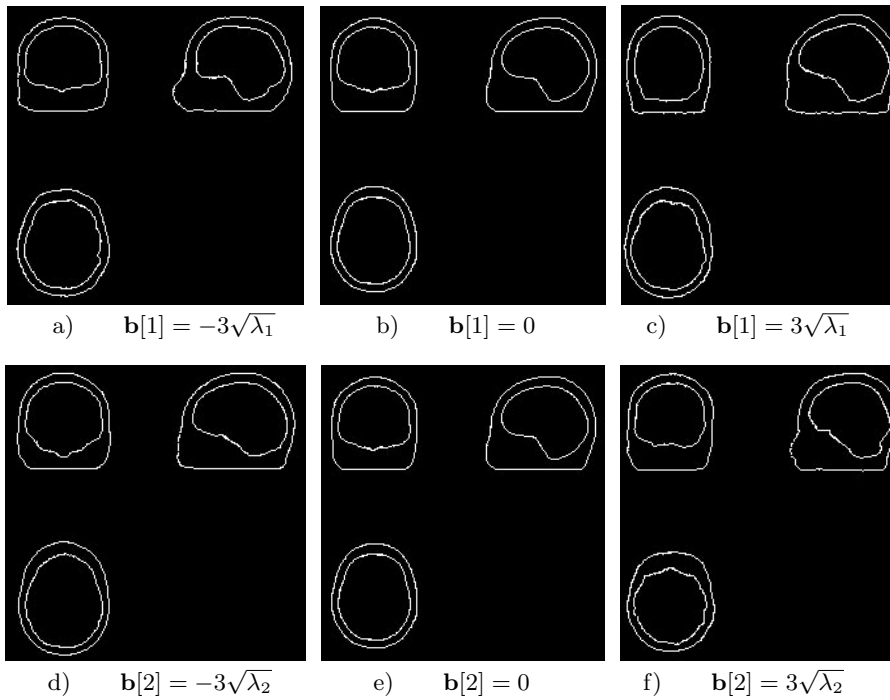

Fig. 2. *Multiplanar view of the 3D joint model's deformations by varying the first two statistical modes in vector* $\mathbf{b}$ *between* $-\sqrt{\lambda_i}$ *and* $\sqrt{\lambda_i}$, $i = 1, 2$. λ_i *designates the* i^{th} *eigenvalue of the covariance matrix* $\mathbf{\Gamma}$.

As it can be seen in Table 1, with the KL representation, only a few parameters are necessary to describe the variations in the training population (fig. 2). Table 1 shows that, for instance 5 parameters carry approximately 95% of the global information.

The number of degrees of freedom of the original mesh, for both head and brain surfaces, was $2 \times 3NN' = 2 \times 3 \times 100 \times 100 = 60000$. In the vibration modes subspace, this number was reduced to $3(M_H + M_B) = 3 \times (2500 + 2500) = 15000$ and finally in the KL subspace the degrees of freedom were reduced to $m \simeq 5$ achieving a compression ratio of 12000 : 1. This compression ratio enables a compact description of shape variability, and results in a tractable constrained deformable model for brain image segmentation and registration, as described in the next section.

Table 1. *Percentage of the global information carried by the different eigenvalues associated with the statistical model. The total number of non-zero eigenvalues is 50.*

KL decomposition of joint model variability

λ_k	$\frac{\lambda_k}{\sum_{i=1}^{50} \lambda_i}$ (%)	$\frac{\sum_{i=1}^{k} \lambda_i}{\sum_{i=1}^{50} \lambda_i}$ (%)
λ_1	51.12	51.12
λ_2	20.54	71.66
λ_3	12.91	84.57
λ_4	7.38	91.95
λ_5	3.16	95.11
$\vdots$	$\vdots$	$\vdots$
λ_{50}	0.00	100.0

4 Applications

Several applications of the statistical model may be considered in brain image processing. The model may be used as a simplified anatomical representation of the images belonging to the training set. If the training set is representative enough of a population, the model may also be used to analyse images of patients not belonging to the training set. To this end, the 50 subjects of our data base were carefully selected, with the aid of an expert neurologist. Besides, the data base is conceived in such a way that it can be incrementally augmented by new elements.

We consider here two applications of the joint statistical model: the segmentation of the brain from 3D MRI and the registration of multimodal (MRI/SPECT) brain images. Before presenting these two applications, let us notice that the equation describing the configuration of the statistical model:

$$\mathbf{X}(\mathbf{b}) = \mathbf{X}_{INIT} + \underline{\overline{\mathbf{\Phi}}}\bar{\mathbf{a}} + \underline{\overline{\mathbf{\Phi}}}\mathbf{P}\mathbf{b} \tag{23}$$

may be separated into two equations describing the head and brain parts of the model:

$$\mathbf{X}_H(\mathbf{b}) = \mathbf{X}_0 + \mathbf{\Phi}_H\bar{\mathbf{a}}_H + \mathbf{\Phi}_H\mathbf{P}_{HB}\mathbf{b} \tag{24}$$

$$\mathbf{X}_B(\mathbf{b}) = \mathbf{X}_0 + \mathbf{\Phi}_B\bar{\mathbf{a}}_B + \mathbf{\Phi}_B\mathbf{P}_{BH}\mathbf{b} \tag{25}$$

Let us also recall that equations (24) and (25) are coupled by the sub-matrices $\mathbf{P}_{HB}$ and $\mathbf{P}_{BH}$ representing the statistical dependencies (spatial relationships) between the two anatomical structures. These submatrices cannot be calculated separately: they are parts of matrix $\mathbf{P}$. The terms $\bar{\mathbf{a}}_H$ and $\bar{\mathbf{a}}_B$ express the mean vibration amplitudes for the head and brain surfaces of the training set, $\mathbf{X}_0$ is the initial spherical mesh and $\mathbf{\Phi}_H$ and $\mathbf{\Phi}_B$ denote its eigenvectors.

4.1 Brain Segmentation

In order to segment the brain from a patient MRI volume, not belonging to the training set, the patient head is first parameterized by the physics-based model. The head structure is easily segmented from its background by simple thresholding and region growing algorithms. The segmented head surface is parameterized by the amplitudes of the vibration modes of a spherical mesh, as already explained in Section 2. The spherical mesh is initialized around the head structure and equation (2) is solved in the modal subpsace. The solution for the vibration amplitudes describing the patient head surface is:

$$\tilde{u}_i^h = \frac{1}{\omega_i^2} \tilde{f}_i^h \tag{26}$$

for $i = 1, ..., 3M_H$. The head surface coordinates are obtained by introducing vector $\tilde{\mathbf{U}}^H = (\tilde{u}_1^h, \tilde{u}_2^h, \ldots, \tilde{u}_{M_H}^h)^T$ in equation (11):

$$\mathbf{X}_H(\tilde{\mathbf{U}}^H) = \mathbf{X}_0 + \mathbf{\Phi}_H \tilde{\mathbf{U}}^H \tag{27}$$

The next step consists in determining the statistical model parameters $\mathbf{b}$ describing "at best" the segmented head surface:

$$\mathbf{X}_H(\mathbf{b}) = \mathbf{X}_0 + \mathbf{\Phi}_H \bar{\mathbf{a}}_H + \mathbf{\Phi}_H \mathbf{P}_{HB} \mathbf{b} = \mathbf{X}_H(\tilde{\mathbf{U}}^H) \tag{28}$$

System (28) is overconstrained: there are $3NN'$ equations (the head surface coordinates $\mathbf{X}_H$) and m unknowns (the components of $\mathbf{b}$). Moreover, matrix $\mathbf{P}_{HB}$, describing the head and brain surfaces spatial relation, constrains vector $\mathbf{b}$ to describe *both* head and brain surfaces. Further regularization may be obtained by adding a strain-energy minimization constrain [15]:

$$E_s = \frac{1}{2} \mathbf{b}^T \mathbf{\Lambda}^2 \mathbf{b} \tag{29}$$

where $\mathbf{\Lambda} = diag\{\lambda_i\}$ contains the eigenvalues of the covariance matrix $\mathbf{\Gamma}$. Strain energy enforces a penalty proportional to the squared eigenvalue associated with each component of $\mathbf{b}$.

The solution of (28) is formulated in terms of minimization of a regularized least squares error:

$$\begin{aligned} E(\mathbf{b}) = {} & [\mathbf{X}_H(\tilde{\mathbf{U}}^H) - \mathbf{X}_0 - \mathbf{\Phi}_H \bar{\mathbf{a}}_H - \mathbf{\Phi}_H \mathbf{P}_{HB} \mathbf{b}]^T [\mathbf{X}_H(\tilde{\mathbf{U}}^H) - \mathbf{X}_0 \\ & - \mathbf{\Phi}_H \bar{\mathbf{a}}_H - \mathbf{\Phi}_H \mathbf{P}_{HB} \mathbf{b}] + \alpha \mathbf{b}^T \mathbf{\Lambda}^2 \mathbf{b} \end{aligned} \tag{30}$$

Differentiating with respect to $\mathbf{b}$, we obtain the strain-minimizing overconstrained least squares solution:

$$\mathbf{b}^* = [(\mathbf{\Phi}_H \mathbf{P}_{HB})^T \mathbf{\Phi}_H \mathbf{P}_{HB} + \alpha \mathbf{\Lambda}^2]^{-1} (\mathbf{\Phi}_H \mathbf{P}_{HB})^T [\mathbf{X}_H(\tilde{\mathbf{U}}^H) - \mathbf{X}_0 - \mathbf{\Phi}_H \bar{\mathbf{a}}_H]. \tag{31}$$

A first estimate of the patient's brain surface is then recovered by introducing the estimated parameter $\mathbf{b}^*$ in equation (25), describing the brain part of the statistical model:

$$\mathbf{X}_B(\mathbf{b}^*) = \mathbf{X}_0 + \mathbf{\Phi}_B \bar{\mathbf{a}}_B + \mathbf{\Phi}_B \mathbf{P}_{BH} \mathbf{b}^* \tag{32}$$

Equation (32) provides *a good initial prediction of the location of the brain surface*, obtained by exploiting the spatial relationships between head and brain, coded in the learned statistical representation. This feature of the proposed approach significantly alleviates the problem of manual initialization which is a requirement in most of the deformable model-based segmentation methods.

Further improvement of this initial solution may be obtained by alternately optimizing an energy function parameterized by the m components of vector $\mathbf{b}$ [5], in order to fit the part of the model describing the brain, $\mathbf{X}_B$, to a noisy contour map I_c extracted from the MRI image [8]. In our case, the cost function E to be optimized is defined as:

$$E(\mathbf{b}) = \sum_{p \in \mathbf{X}_B(b)|p=1}^{3NN'} \nabla_G * I_c(p) \tag{33}$$

where the operator ∇_G denotes the gradient of a Gaussian kernel. The above cost function simply counts the number of points of the model located on a contour point of the smoothed brain image. Optimization of energy function (33) is obtained by a non linear Gauss-Seidel like algorithm, known as ICM [2]. It has fast convergence properties and only accepts configurations decreasing the cost function.

To summarize, the overall segmentation algorithm is based on the following steps:

1. Parameterization of the head surface using equations (26) and (27).
2. Estimation of the statistical deformation parameters $\mathbf{b}^*$ by solving the regularized overconstrained system (31).
3. Prediction of the brain surface by equation (32).
4. Fine-tuning of the solution by deterministic optimization of cost function (33).

Figure 3 presents a typical example of brain segmentation from a 3D MRI, corresponding to a patient not belonging to the training set. The image in figure 3(a) is a post-operative MRI (thus exhibiting missing data). In figure 3(b) the head surface is segmented and parameterized by the physics-based deformable model (eq. (26) and (27)). In fig. 3(b), the head surface coordinates combined with the probabilistic model provide a good prediction for the brain surface. The statistical model is not affected by missing data because its deformations are constrained by the statistical analysis of the shape variations observed in the training population. The whole segmentation process takes about 5 min cpu time on a standard (HP 9000/C200) workstation for a 128^3 image volume. Most of the computation time concerns head surface parameterization and especially the image forces based on the euclidean distance transform of the 3D MR image [3].

4.2 Multimodal Image Registration

The second application considered in this paper concerns the rigid registration of multimodal (MR/SPECT) 3D images. Registration of a multimodal image

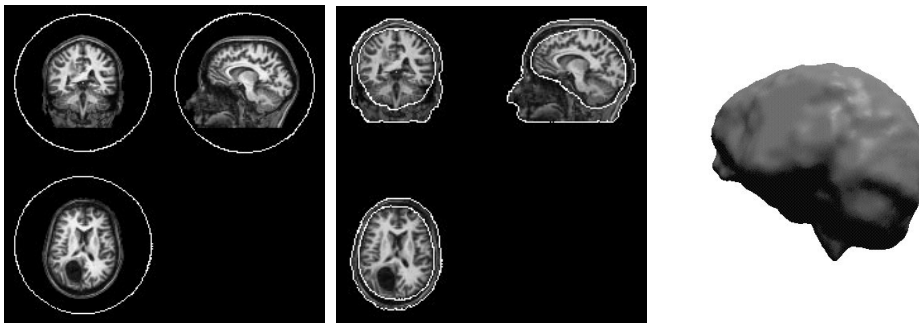

a) b) c)

Fig. 3. **(a)** *A patient MR image with the initial spherical mesh superimposed.* **(b)** *Prediction of the brain surface using the head surface and the probabilistic deformable model.* **(c)** *3D rendering of the segmented brain.*

pair consists in estimating the rigid transformation parameters (3D rotation and translation parameters) that have to be applied to the image to be registered (here the SPECT image) in order to match the reference image (here the MRI).

The registration relies on the head structure in the MRI and the brain structure in the SPECT image, which are easy to extract from these two modalities (contrary to the brain structure in MRI). These structures do not overlap but the deformable model represents the relative location of the head and brain contours and accounts for the anatomical variability observed among the training population. The deformable model (restricted here to head and brain surfaces) is used as a probabilistic atlas that constrains the rigid registration of the image pair.

The multimodal rigid registration method relies on the following steps:

1. Segmentation of the head structure in MRI and the brain structure in SPECT from their backgrounds.
2. Brain surface recovery from the MRI using the segmentation algorithm presented in section 4.1
3. Registration of the estimated brain surface with the SPECT brain surface by optimization of a cost function.

The first step is standard preprocessing for background noise elimination. The second step estimates the brain surface from the MRI using the head surface parameterization and the statistical deformable model. By these means, multimodal image registration is also a measure for the accuracy of the segmentation process. Finally, the third step brings into alignment the estimated MRI brain surface and the SPECT image surface by optimization of an objective function having as variables the rigid transformation parameters between the two surfaces. Various cost functions may be used in that step for the registration of

binary surfaces. We have applied the following energy function:

$$E(\Theta) = \sum_{p \in I_{SPECT}} I_D(T_\Theta(p)) \tag{34}$$

where T_Θ is the rigid transformation with parameters $\Theta = \{t_x, t_y, t_z, \theta_x, \theta_y, \theta_z\}$, p is a voxel of the SPECT image surface I_{SPECT} and I_D is the chamfer distance transformation [3] of the part of the statistical model describing the brain. For all of the SPECT surface voxels, equation (34) counts the distance between a SPECT image surface point and its nearest point on the deformable model surface. We have chosen chamfer distance matching because it is fast and it is easily generalized to any surfaces. The whole registration procedure takes about 10 min cpu time on a HP C200 workstation for a 128^3 image volume.

Figure 4 shows an example of a MRI/SPECT registration using the proposed technique. The images in figure 4(a) show the two volumes before registration. The SPECT contours are superimposed onto the MRI to qualitatively evaluate the registration. Figure 4(b) presents the head and brain surface recovery of the MRI using the segmentation algorithm described in the previous section. The matching of the SPECT volume to the part of the model describing the brain is illustrated in fig.4(c). The images in figure 4(d) show the two volumes after registration. As can be seen, although the MRI and SPECT head and brain contours do not overlap, the two images have been correctly registered using the statistical model.

To quantitatively assess the ability of the physics-based statistical deformable model to handle multimodal image pairs, a 3D SPECT image volume has been manually registered to its corresponding MRI volume with the aid of an expert physician. The manually registered SPECT volume was then transformed using translations between -20 and $+20$ voxels and rotations between -30 and $+30$ degrees. By these means 25 new images were created. These images were then registered using three different techniques and statistics on the registration errors were computed on the set of 25 different registrations. We have compared our Statistical Deformable Model-based technique (SDM) to the maximization of the Mutual Information (MI) [6] (currently considered as a reference method) and the Robust Inter-image Uniformity criterion (RIU) developed by the authors [11, 12]. Both of the latter techniques have been validated in previous studies and are robust to missing data, outliers and large rotations. For each method, the estimated registration parameters, that is the 3D translations (t_x, t_y, t_z) and rotations (θ_x, θ_y, θ_z) were compared to the true ones to determine the accuracy of the registration. Tables 2 and 3 show the mean, the standard deviation, the median and maximum of the registration errors for the different techniques. As can be seen the proposed SDM approach leads to a registration accuracy which is close to the two other methods.

5 Conclusion and Future Prospects

We have presented a physically-based 3D statistical deformable model embedding information on the spatial relationships and anatomical variability of mul-

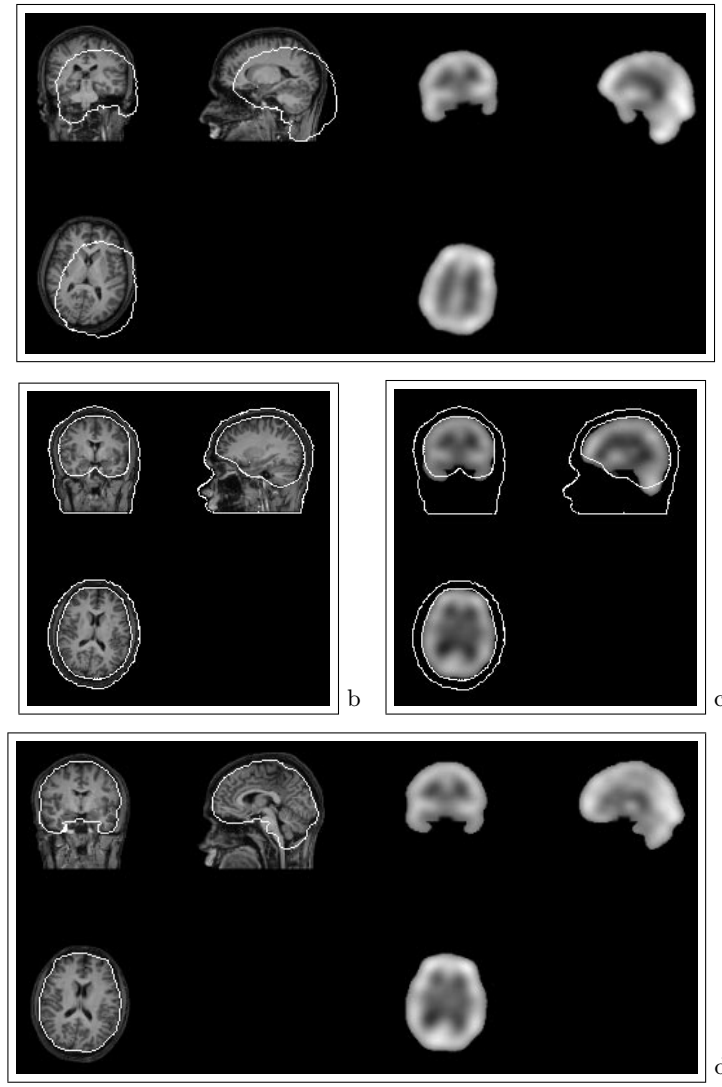

Fig. 4. *MRI/SPECT registration using the deformable model.* **(a)** *MRI and SPECT volumes before registration. The SPECT contours are superimposed onto the MRI to illustrate the misalignment.* **(b)** *Parameterization of the head structure and estimation of the brain surface of the MR image in* **(a)** *using the statistically constrained deformable model.* **(c)** *Registration of the SPECT image to the part of the statistical model describing the brain surface.* **(d)** *MRI and SPECT volumes after registration. The registered SPECT image contours are superimposed onto the MRI to illustrate the alignment of the two images.*

Table 2. *Multimodal registration of 3D MRI/SPECT images. A 3D SPECT image volume manually pre-registered by an expert to its MRI counterpart was artificially transformed using 25 different translation and rotation parameters. The average and the standard deviation of the registration errors are presented for the different methods. Translation errors are given in voxels and rotation errors in degrees.*

3D MRI/SPECT Registration Errors ($\mu \pm \sigma$)

	MI	RIU	SDM
Δt_x	1.33 ± 1.16	$0.47 \pm 0,41$	0.89 ± 0.43
Δt_y	1.61 ± 1.06	$1.13 \pm 0,90$	0.86 ± 0.88
Δt_z	1.06 ± 1.19	$1.08 \pm 0,74$	1.05 ± 1.02
$\Delta \theta_x$	1.26 ± 1.09	$0.75 \pm 0,56$	1.15 ± 1.11
$\Delta \theta_y$	1.60 ± 0.92	$0.58 \pm 0,44$	1.28 ± 0.87
$\Delta \theta_z$	0.99 ± 0.86	$1.04 \pm 0,78$	1.29 ± 0.67

Table 3. *Multimodal registration of 3D MRI/SPECT images. A 3D SPECT image volume manually pre-registered by an expert to its MRI counterpart was artificially transformed using 25 different translation and rotation parameters. The median and maximum registration errors for the rigid transformation parameters are presented. See text for technique abbreviations.*

3D MRI/SPECT Registration Errors

	MI	RIU	SDM
median(Δt)	1.35	0.63	0.54
maximum(Δt)	4.24	3.05	2.63
median($\Delta \theta$)	1.14	0.52	1.09
maximum($\Delta \theta$)	4.35	2.47	3.52

tiple anatomical structures, as observed over a representative population. The particular model developed in this paper was devoted to head and brain representation. Applications of this model included the registration of multimodal image pairs (MRI/SPECT) and the unsupervised segmentation of the brain structure from a given modality (MRI). The major advantage of statistical models is that they naturally introduce *a priori* statistical knowledge that provides useful constraints for ill-posed image processing tasks, such as image segmentation. Consequently they are less affected by noise, missing data or outliers. As an example, the statistical deformable model was applied to the segmentation of the brain structure from post operative images, in which missing anatomical structures lead standard voxel-based techniques to erroneous segmentations. The registration of multimodal brain images was also handled without performing any preprocessing to remove non-brain structures.

One perspective of our work is to extend the model by representing other anatomical structures of the brain (ventricles, corpus callosum, hippocampus, etc.). The statistical deformable model presented in this paper may be considered as a first step towards the development of a general purpose probabilistic anatomical atlas of the brain.

References

1. K. J. Bathe. *Finite element procedures.* Prentice Hall, Englewood Cliffs, New Jersey, 1996.
2. J. Besag. On the statistical analysis of dirty pictures. *Journal of the Royal Statistical Society*, 48(3):259–302, 1986.
3. G. Borgefors. On digital distance transforms in three dimensions. *Computer Vision and Image Understanding*, 64(3):368–376, 1996.
4. T. F. Cootes, C. J. Taylor, and J. Graham. Active shape models - their training and application. *Computer Vision and Image Understanding*, 1(1):38–59, 1995.
5. C. Kervrann and F. Heitz. A hierarchical Markov modeling approach for the segmentation and tracking of deformable shapes. *Graphical Models and Image Processing*, 60(3):173–195, 1998.
6. F. Maes, A. Collignon, D. Vandermeulen, G. Marchal, and P. Suetens. Multimodality image registration by maximization of mutual information. *IEEE Transactions on Medical Imaging*, 16(2):187–198, 1997.
7. T. Mc Inerney and D. Terzopoulos. Deformable models in medical image analysis: a survey. *Medical Image Analysis*, 2(1):91–108, 1996.
8. O. Monga and R. Deriche. 3D edge detection using recursive filtering. *Computer Vision and Image Understanding*, 53(1):76–87, 1991.
9. O. Musse, J. P. Armspach, I. J. Namer, F. Heitz, F. Hennel, and D. Grucker. Data-driven curvilinear reconstruction of 3D MRI: application to cryptogenic extratemporal epilepsy. *Magnetic Resonance Imaging*, 16(10):1227–1235, 1998.
10. C. Nastar and N. Ayache. Frequency-based nonrigid motion analysis: Application to four dimensional medical images. *IEEE Transactions on Pattern Analysis and Machine Intelligence*, 18(11):1069–1079, 1996.
11. C. Nikou, J. P. Armspach, F. Heitz, I.J. Namer, and D. Grucker. MR/MR and MR/SPECT registration of brain images by fast stochastic optimization of robust voxel similarity measures. *Neuroimage*, 8(1):30–43, 1998.
12. C. Nikou, F. Heitz, and J. P. Armspach. Robust registration of dissimilar single and multimodal images. In *Lecture Notes in Computer Science. Proceedings of the* 5th *European Conference on Computer Vision (ECCV'98)*, volume 2, pages 51–65, Freiburg, Germany, 2-6 June 1998.
13. A. Pentland and S. Sclaroff. Closed-form solutions for physically-based shape modeling and recognition. *IEEE Transactions on Pattern Analysis and Machine Intelligence*, 13(7):730–742, 1991.
14. G. Székely, A. Keleman, A. Brechbuhler, and G. Gerig. Segmentation of 2D and 3D objects from MRI data using constrained elastic deformations of flexible Fourier contour and surface models. *Medical Image Analysis*, 1(1):19–34, 1996.
15. D. Terzopoulos. The computation of visible surface representations. *IEEE Transactions on Pattern Analysis and Machine Intelligence*, 10(4):417–438, 1988.